A Turn-On Bis-Hydrazone Fluorescent Chemosensor for Selective Cd^{2+} Detection: Synthesis, Structural Insights, and Theoretical Validation

Suman Adhikari[a*], Sourav Nath[a,b], Koushik Saha[c], Nabajyoti Baildya[d], Werner Kaminsky[e], Malavika S Kumar[f], Subhadip Roy[g], Avijit Kumar Das[f*]

[a]*Department of Chemistry, Govt. Degree College, Dharmanagar, Tripura(N)-799253, India.*

[b]*Department of Chemistry and Vivekananda Centre for Research, Ramakrishna Mission Residential College, Narendrapur, Kolkata-700103, India.*

[c]*Department of Chemistry, Jadavpur University, Kolkata 700032, West Bengal, India.*

[d]*Department of Chemistry, Milki High School, Milki, Malda-732209, India.*

[e]*Department of Chemistry, University of Washington, Seattle, Washington 98195, United States*

[f]*Department of Chemistry, Christ University, Hosur Road, Bangalore, Karnataka, 560029 India*

[g]*Department of Chemistry, The ICFAI University Tripura, Kamalghat, Mohanpur, Agartala, 799210, Tripura, India.*

Experimental

X-ray Crystallography

A colorless prism, measuring 0.30 x 0.12 x 0.06 mm^3 was mounted on a loop with oil. Data was collected at -143°C on a Nonius Kappa CCD FR590 single crystal X-ray diffractometer, Mo-radiation. Crystal-to-detector distance was 40 mm and exposure time was 60 seconds per degree for all sets. The scan width was 1°. Data collection was 99.8% complete to 25° in ϑ. A total of 30813 partial and complete reflections were collected covering the indices, -26<=h<=26, -11<=k<=11, -14<=l<=14. A total of 8376 merged and 2360 symmetry independent reflections were collected. The data was integrated and scaled using hkl-SCALEPACK [1]. This program applies a multiplicative correction factor (S) to the observed intensities (I) and has the following form:

$$S = (e^{-2B(\sin^2\theta)/\lambda^2}) / \text{scale}$$

S is calculated from the scale and the B factor determined for each frame and is then applied to I to give the corrected intensity (I_{corr}). Solution by direct methods (SHELXT) [2] produced a complete heavy atom phasing model consistent with the proposed structure. The structure was completed by difference Fourier synthesis with SHELXL [3, 4] Scattering factors are from Waasmair and Kirfel [5]. Hydrogen atoms were placed in geometrically idealised positions and constrained to ride on their parent atoms with C–H distances in the range 0.95-1.00 Angstrom. Isotropic thermal parameters U_{eq} were fixed such that they were $1.2U_{eq}$ of their parent atom Ueq for CH's and $1.5U_{eq}$ of their parent atom U_{eq} in case of methyl groups. All non-hydrogen atoms were refined anisotropically by full-matrix least-squares.

Experimental for fluorescence studies

For fluorescence titration experiments, a stock solution of the probe L (2.0×10^{-5} M) was prepared in a CH_3CN–HEPES buffer mixture (9:1, v/v) at pH 7.4 and 25 °C. Stock solutions of potential interfering metal ions (Al^{3+}, Cd^{2+}, Fe^{3+}, Fe^{2+}, Hg^{2+}, Co^{2+}, Mn^{2+}, Cu^{2+}, Ni^{2+}, Pb^{2+}, and Zn^{2+}) were prepared separately at a concentration of 2.0×10^{-4} M. Initially, the sensor solution was prepared by dissolving probe **1** in 2 mL of acetonitrile, followed by the gradual addition of the corresponding guest analytes in increasing concentrations. Solutions containing a fixed concentration of the

sensor and varying concentrations of analytes were prepared individually, and their fluorescence spectra were recorded accordingly.

Theoretical Methods

Geometry optimization of the bis hydrazone-based probe **1** and Cd(II) complex was performed by applying density functional theory using Gaussian 09 [6]. B3LYP hybrid functional [7] with 6-31+G(d) basis set for non-metal and LANL2DZ basis set with effective core potential for metal (Cd) was applied to offer the precise geometry of the crystal. The UV-Vis spectra with 30 singlet excitations were performed for the bis hydrazone-based probe **1** and Cd(II) complex. The structure of the complex was confirmed by frequency calculations to their true minima.

Topological analysis of the crystal packing

Taking into account all intermolecular contacts during simplification procedure, one can obtain a description of the molecular packing. Using the subroutine implemented in ToposPro, different subnets can be obtained from the underlying net that contains the edges of a weight no less than a specified value. The standard representation of the Coulomb or vdW-bonded structure resulted in the 2-nodal net of the unknown topological type with point symbol for net: $\{3^{18}.4^{10}\}_2\{3^{90}.4^{214}.5^{73}.6\}$ (**Fig. S5**).

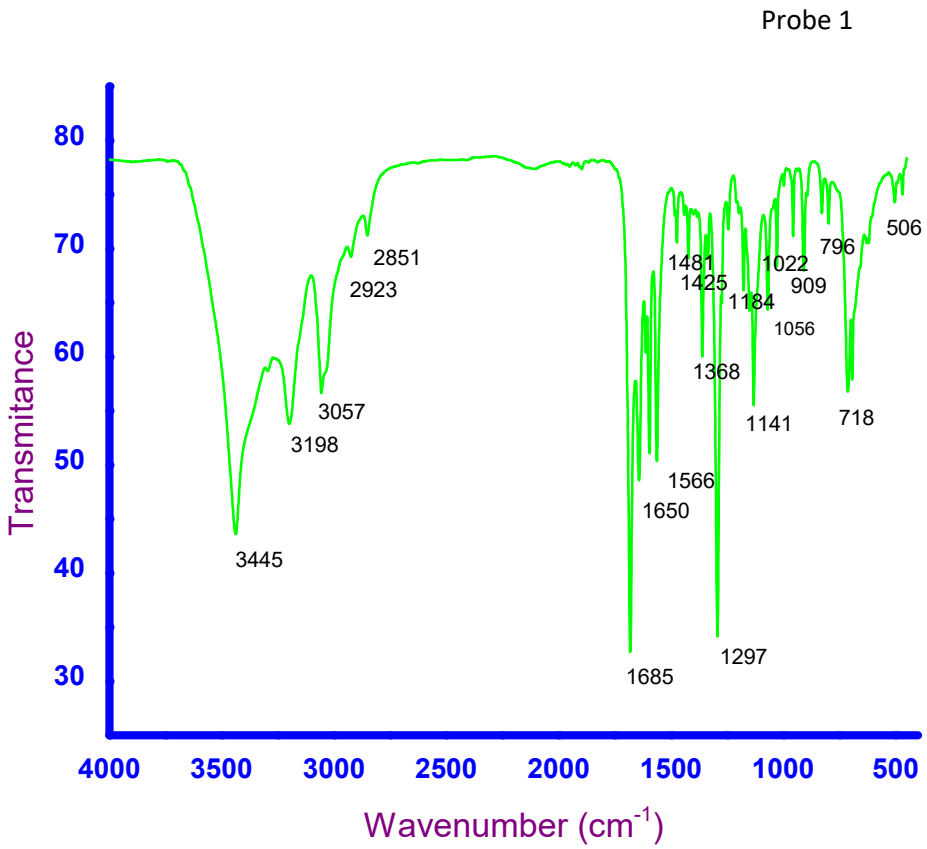

Fig. S1. FT-IR spectrum of bis hydrazone-based probe **1**.

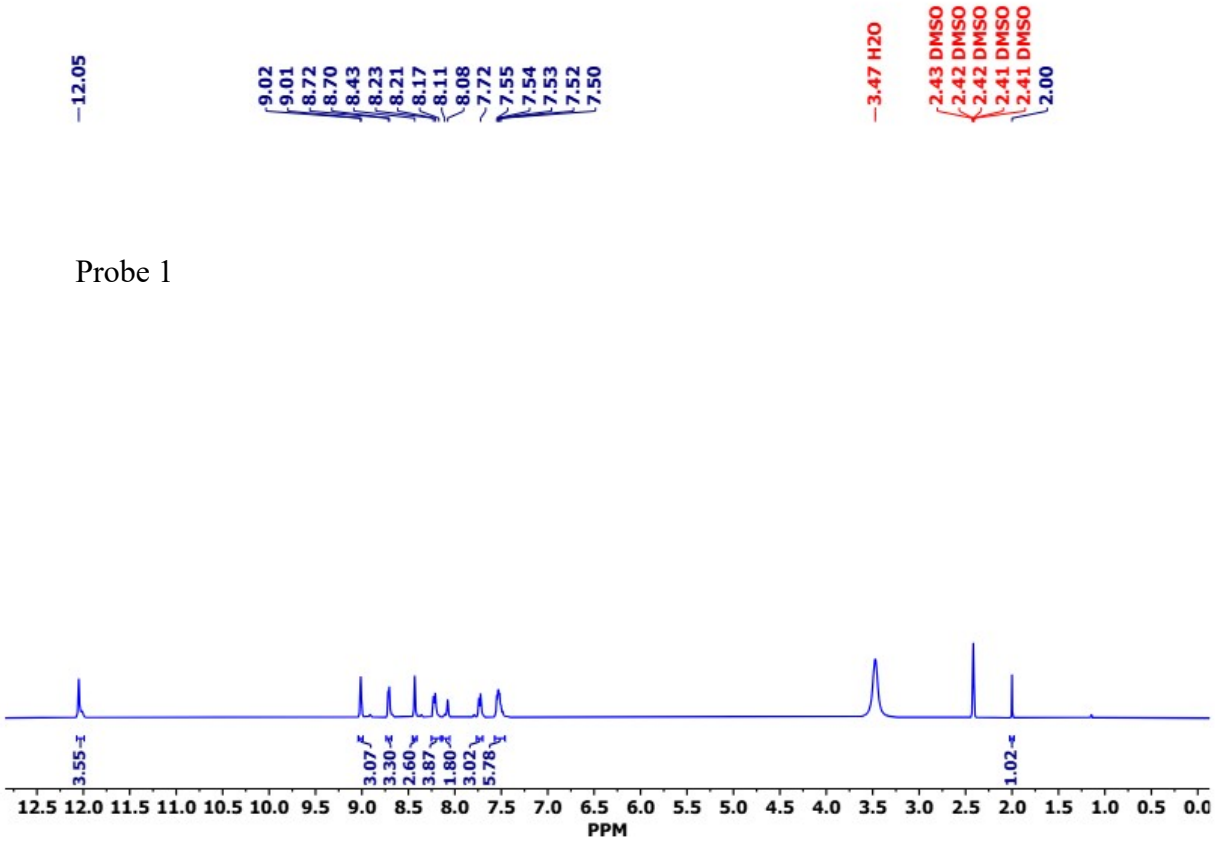

Probe 1

Fig. S2. ^{1}H NMR spectrum of bis hydrazone-based probe **1** in DMSO-d_6.

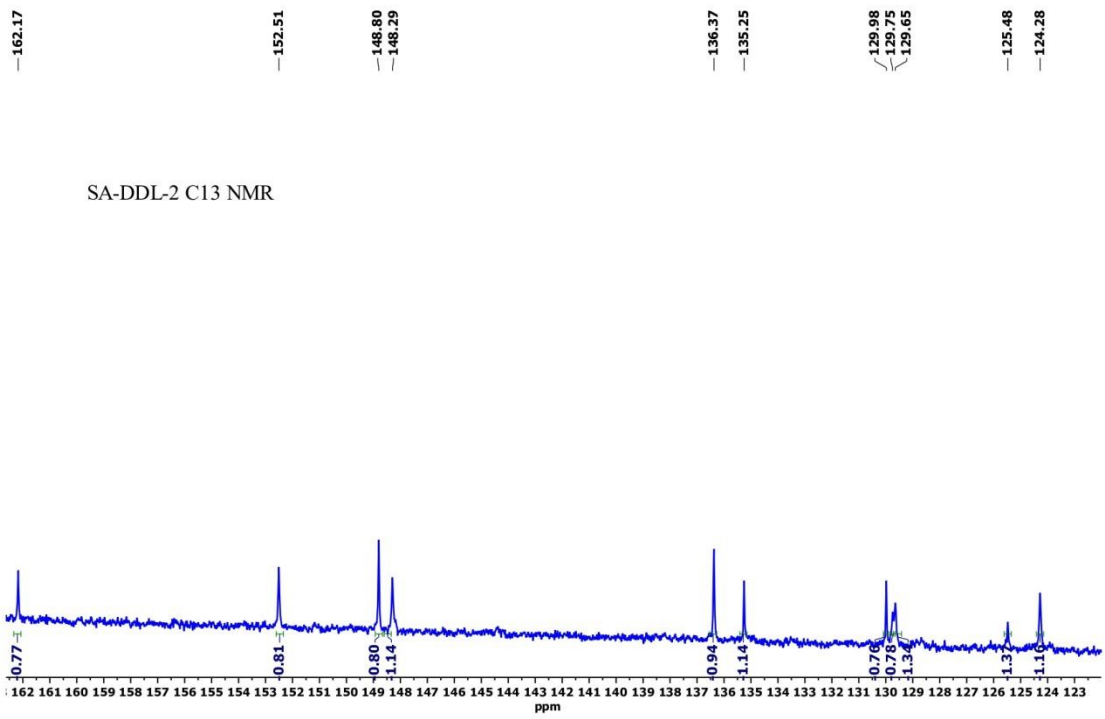

Fig. S3. ^{13}C NMR spectrum of bis hydrazone-based probe **1** in DMSO-d_6.

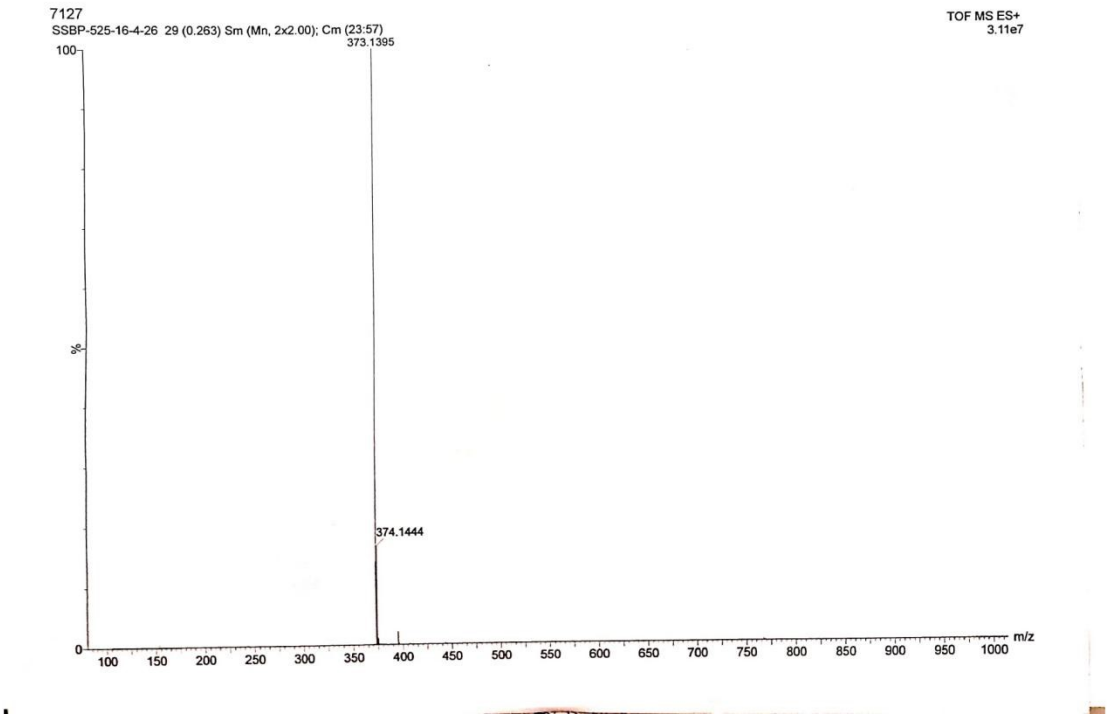

Fig. S4. HRMS of bis hydrazone-based probe **1.**

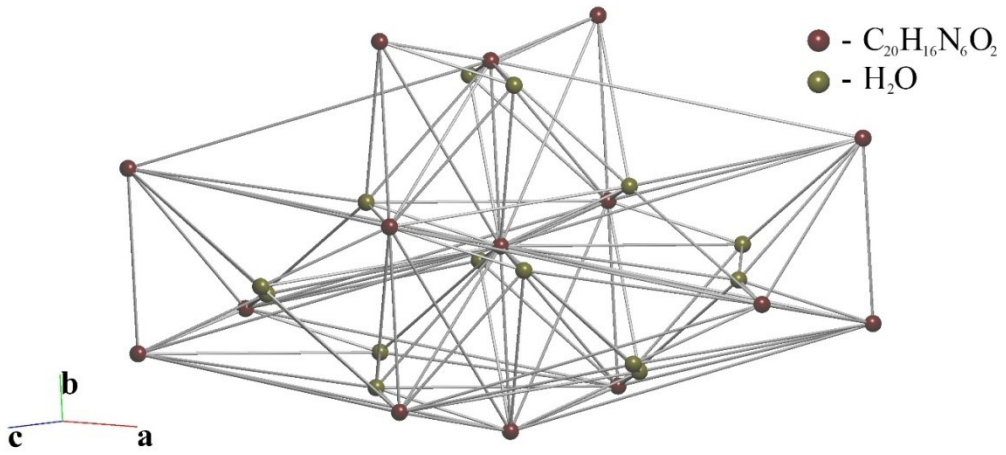

Fig. S5. 8,28-c net in standard representation of Coulomb or vdW-bonded molecular structure.

Having applied the multilevel analysis, we obtain the following order of the subnets that describe the packing of the structure on different levels of solid angle (Ω_i, %) (**Table S4**). **Fig. S5** presents the formation of a 8,28-c net depending on the value of the solid angle. This is a possible mechanism for the formation of the final structure.

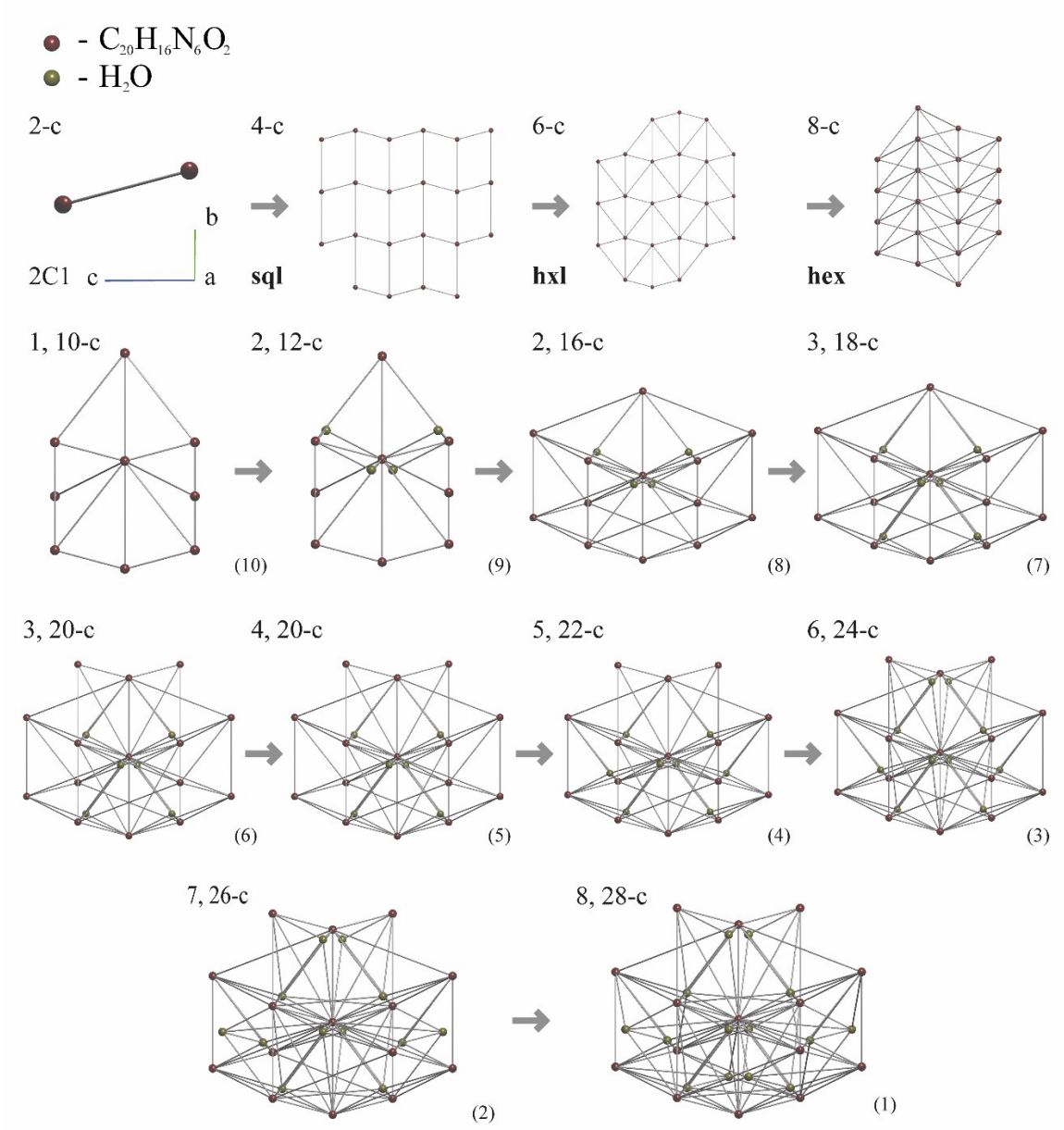

Fig. S6. Order of the subnets that describe the packing of the structure on different levels of Ω_i.

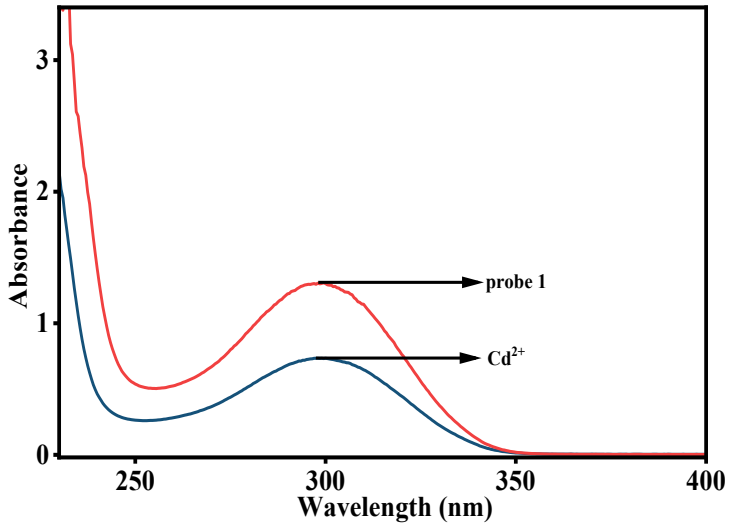

Fig. S7. UV-*Vis* spectra of probe **1** (c = 20 μM) (red line) and probe 1 with Cd^{2+} (c = 200 μM) (blue line).

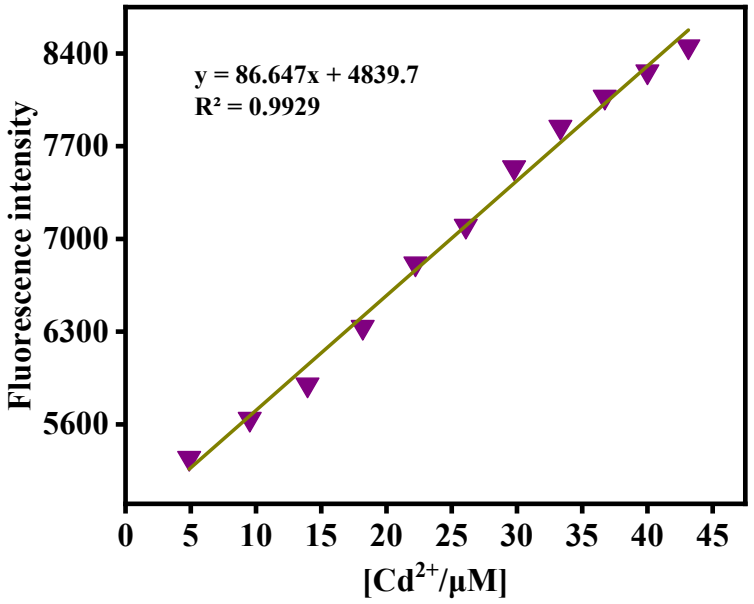

Fig. S8. Changes of fluorescence intensity of probe **1** as a function of [Cd^{2+}] at 420 nm.

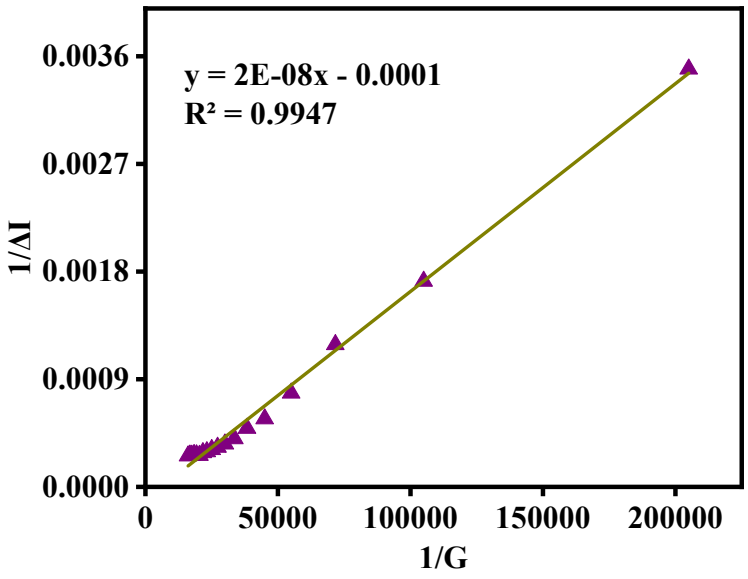

Fig. S9. Benesi–Hildebrand plot from fluorescence titration data of probe **1** (c = 20 μM) with Cd^{2+}.

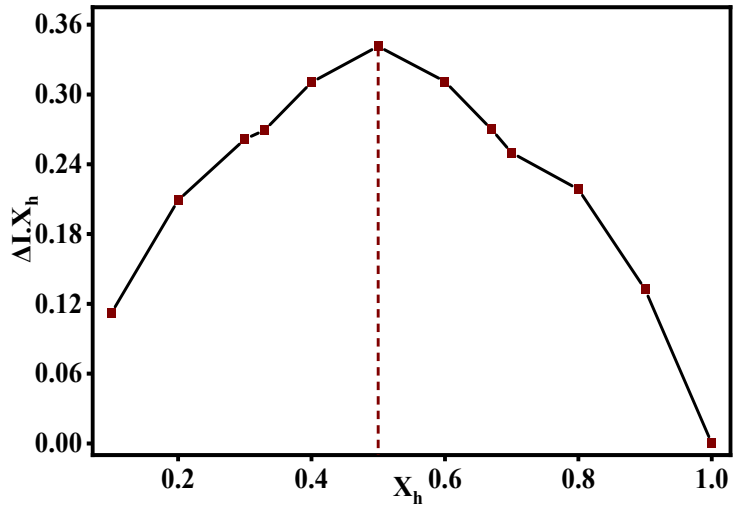

Fig. S10. Jobs plot analysis of probe **1** with Cd^{2+}

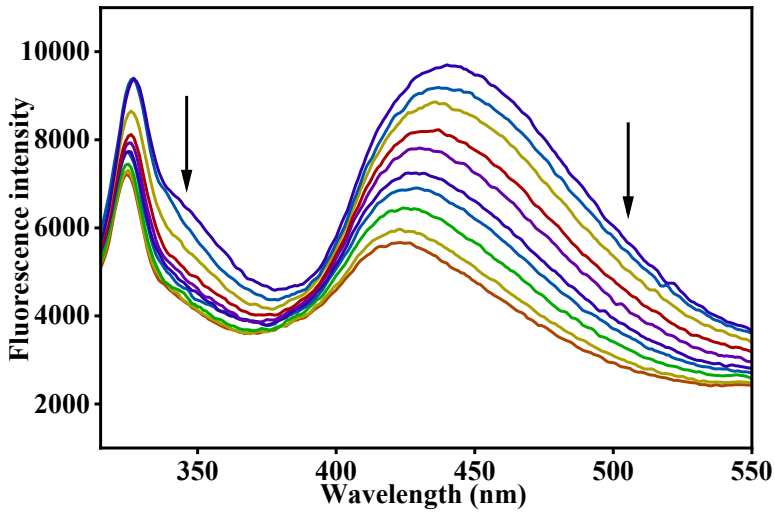

Fig. S11. Reversibility studies of probe **1**-Cd^{2+} with EDTA.

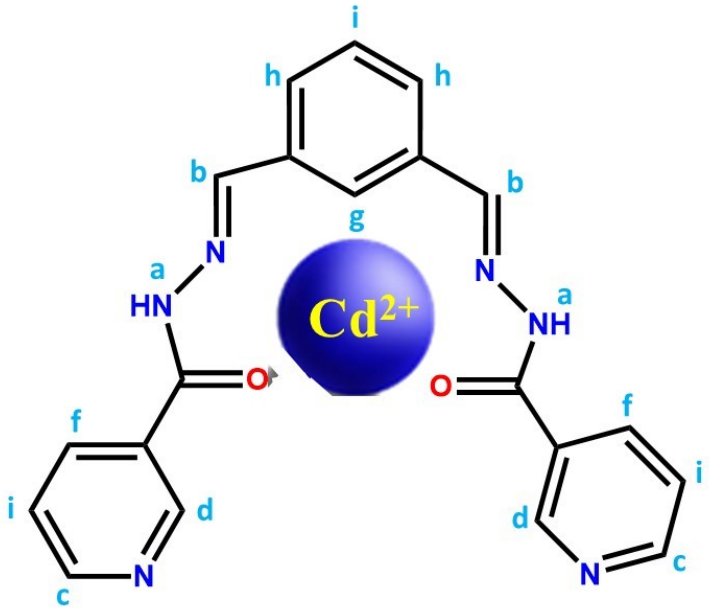

Fig. S12. Probable binding interactions of probe **1** with Cd^{2+}.

Table S1. Crystal data and structure refinement for probe **1.**	
Identification code	**1**
Empirical formula	$C_{20}H_{20}N_6O_4$
Formula weight	408.420
Temperature/K	100.15
Crystal system	monoclinic
Space group	C2/c
a/Å	19.9418(11)
b/Å	8.6405(3)
c/Å	11.5476(5)
α/°	90
β/°	104.228(6)
γ/°	90
Volume/Å^3	1928.70(16)
Z	4
ρ_{calc}g/cm^3	1.407
μ/mm^{-1}	0.102
F(000)	856.6
Crystal size/mm^3	0.3 × 0.12 × 0.06
Radiation	Mo Kα (λ = 0.71073)
2θ range for data collection/°	4.22 to 56.54
Index ranges	$-26 \leq h \leq 26$, $-11 \leq k \leq 11$, $-14 \leq l \leq 14$
Reflections collected	8376
Independent reflections	2360 [R_{int} = 0.0812, R_{sigma} = 0.0672]
Data/restraints/parameters	2360/0/149
Goodness-of-fit on F^2	1.007
Final R indexes [I≥ 2σ (I)]	R_1 = 0.0485, wR_2 = 0.1128
Final R indexes [all data]	R_1 = 0.0874, wR_2 = 0.1332
Largest diff. peak/hole / e Å^{-3}	0.49/-0.51

Table S2. Bond lengths for probe **1.**

Atom	Atom	Length/Å		Atom	Atom	Length/Å
C1	C2[1]	1.387(2)		C6	O1	1.2332(18)
C1	C2	1.387(2)		C7	C8	1.395(2)
C2	C3	1.398(2)		C7	C11	1.390(2)
C3	C4[1]	1.3964(19)		C8	C9	1.389(2)
C3	C5	1.470(2)		C9	C10	1.377(2)
C5	N1	1.276(2)		C10	N3	1.340(2)
C6	C7	1.499(2)		C11	N3	1.337(2)
C6	N2	1.355(2)		N1	N2	1.3854(18)

[1]1-X,+Y,1/2-Z

Table S3 Bond angles for probe **1.**

Atom	Atom	Atom	Angle/°	Atom	Atom	Atom	Angle/°
C2	C1	C2[1]	119.9(2)	C8	C7	C6	125.16(15)
C3	C2	C1[1]	120.49(16)	C11	C7	C6	116.97(14)
C4[1]	C3	C2	119.27(15)	C11	C7	C8	117.87(15)
C5	C3	C2	119.70(14)	C9	C8	C7	118.34(15)
C5	C3	C4[1]	121.01(15)	C10	C9	C8	118.97(15)
C3	C4	C3[1]	120.5(2)	N3	C10	C9	124.01(15)
N1	C5	C3	120.07(14)	N3	C11	C7	124.41(16)
N2	C6	C7	117.50(14)	N2	N1	C5	116.44(13)
O1	C6	C7	119.95(14)	N1	N2	C6	117.17(13)
O1	C6	N2	122.55(14)	C11	N3	C10	116.39(15)

[1]1-X,+Y,1/2-Z

Table S4. Multilevel analysis of **1.**

No.	Node degrees	Ω_i, %	Dimensionality of net	Topological type
1	8,28-c	0.21	3D	New topology with point symbol $\{3^{18}.4^{10}\}_2\{3^{90}.4^{214}.5^{73}.6\}$
2	7,26-c	0.26	3D	New topology with point symbol $\{3^{13}.4^{7}.5\}_2\{3^{76}.4^{188}.5^{59}.6^{2}\}$
3	6,24-c	1.17	3D	New topology with point symbol $\{3^{66}.4^{160}.5^{49}.6\}$ $\{3^{9}.4^{4}.5^{2}\}_2$
4	5,22-c	1.26	3D	New topology with point symbol $\{3^{54}.4^{124}.5^{51}.6^{2}\}$ $\{3^{6}.4^{3}.5\}_2$
5	4,20-c	1.40	3D	New topology with point symbol $\{3^{3}.4^{2}.5\}_2\{3^{42}.4^{104}.5^{43}.6\}$
6	3,20-c	2.56	3D	New topology with point symbol $\{3^{3}\}_2\{3^{42}.4^{100}.5^{47}.6\}$
7	3,18-c	2.72	3D	New topology with point symbol $\{3^{36}.4^{72}.5^{42}.6^{3}\}\{3^{3}\}_2$
8	2,16-c	3.37	3D	New topology with point symbol $\{3^{28}.4^{54}.5^{30}.6^{8}\}\{3\}_2$
9	2,12-c	3.37	3D	New topology with point symbol $\{3^{10}.4^{28}.5^{19}.6^{9}\}\{3\}_2$
10	1,10-c	4.02	3D	New topology with point symbol $\{0\}_2\{3^{6}.4^{18}.5^{3}.6\}$
11	8-c	4.25	3D	hex
12	6-c	4.60	2D	hxl
13	4-c	7.53	2D	sql
14	2-c	11.30	1D	2C1

Table S5: Hydrazone-based sensors for the detection of Cd^{2+} ions.

Probe	Guest	Sensing techniques	Sensor type	Binding constant	LOD	References
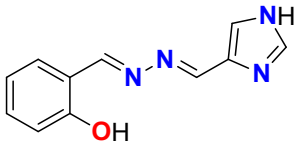	Cd^{2+} and F^-	UV–vis, fluorescence titrations.	turn-on	3.8×10^{-2} M (UV-Vis method) 5.6×10^{-2} M (Fluorescence method)	0.4×10^{-10} M	[8]
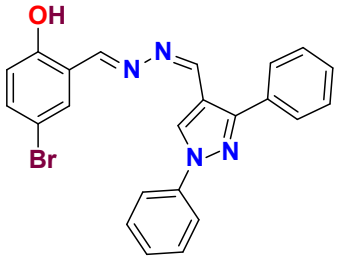	Cd^{2+}, Zn^{2+} and F^-	UV–vis, fluorescence titrations.	turn-on	6.81×10^{-4} M (UV-Vis method) 8.3×10^{-5} M (Fluorescence method)	0.01 nM	[9]
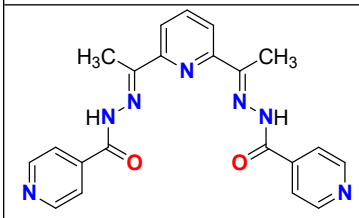 A 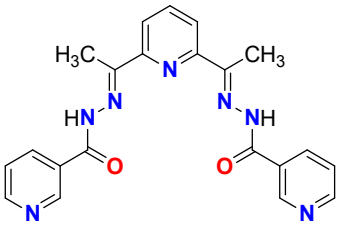 B	Cd^{2+}	UV–vis, fluorescence titrations,	"turn-off for A and B turn-on for C	Not reported	5.05×10^{-5} M, 4.66×10^{-5} M and 8.5×10^{-6} M	[10]

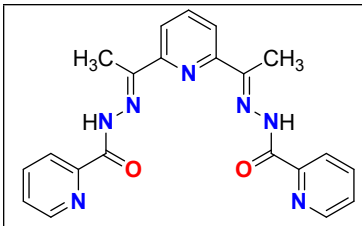 **C**						
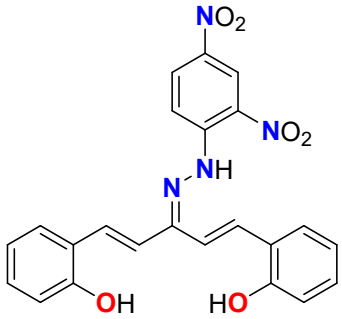	Hg^{2+}, Fe^{2+}, Pb^{2+}, and Cd^{2+}	UV–vis,	-	Not reported	0.75 nM	[11]
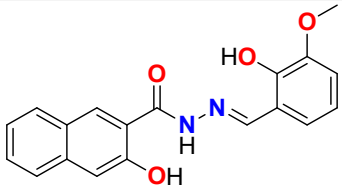	Cd^{2+} and Zn^{2+}	fluorescence titrations	turn-on	2.61×10^{12} M^{-3}	0.13 μM	[12]
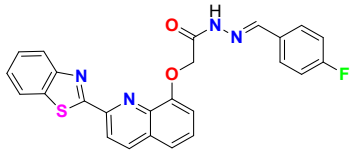	Cd^{2+}	UV–vis, fluorescence titrations,	-	5.21×10^{4} M^{-1} (Fluorescence method)	68 nM	[13]
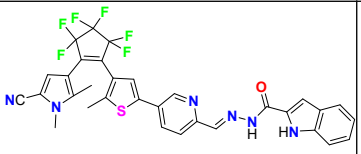	Cd^{2+} and Zn^{2+}	UV–vis, fluorescence titrations,	turn-on	4.36×10^{4} L mol^{-1}	5.74×10^{-7} mol L^{-1}	[14]
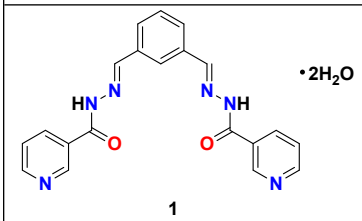 **1**	Cd^{2+}	UV–vis, fluorescence titrations,	turn-on	5×10^{3} M^{-1} (Fluorescence method)	3.39 μM	This work

References

1. Otwinowsky, Z.; Minor, W. In: Methods in Enzymology; Carter, C. W., Jr., Sweet, R. M., Eds.; Academic Press: New York, 1997, 276, 307-326.

2. Sheldrick GM. (2015) SHELXT - Integrated space-group and crystal-structure determination. Acta Cryst. A71, 3-8. https://journals.iucr.org/a/issues/2015/01/00/sc5086/index.html

3. Sheldrick GM. (1997) SHELXL-97, Program for the Refinement of Crystal Structures. University of Göttingen, Germany.

4. Sheldrick GM. (2015) Crystal structure refinement with SHELXL. Acta Cryst. (2015). C71, 3–8. https://journals.iucr.org/c/issues/2015/01/00/fa3356/index.html

5. Waasmaier, D.; Kirfel, A. Acta Crystallogr. A. 1995, **51**, 416. https://journals.iucr.org/paper?sh0059

6. Hiscocks, J., & Frisch, M. J. (2009). Gaussian 09: IOps Reference (pp. 1-170). M. Caricato, & M. J. Frisch (Eds.). Wallingford, CT, USA: Gaussian.

7. Qian, X., Zhu, Y. Z., Song, J., Gao, X. P., & Zheng, J. Y. (2013). New donor-π-acceptor type triazatruxene derivatives for highly efficient dye-sensitized solar cells. *Organic letters*, *15*(23), 6034-6037. https://doi.org/10.1021/ol402931u.

8. Karuppiah, K., Malini, N., Chinnamadhaiyan, M., Yesudhasan, C., Sepperumal, M., Rajabathar, J. R., ... & Selvaraj, M. (2023). A novel hydrazone platform for the recognition of Cd2+ and F− ions: Imaging analysis in Zebrafish embryos. *Journal of Molecular Structure*, *1282*, 135152. https://doi.org/10.1016/j.molstruc.2023.135152.

9. Krishnaveni, K., Murugesan, S., & Siva, A. (2021). Fluorimetric and colorimetric detection of multianalytes Zn2+/Cd2+/F− ions via 5-bromosalicyl hydrazone appended pyrazole receptor; live cell imaging analysis in HeLa cells and zebra fish embryos. Inorganic Chemistry Communications, 132, 108843. https://doi.org/10.1016/j.inoche.2021.108843.

10. Danilescu, O., Bourosh, P., Kulikova, O. V., Chumakov, Y. M., Bulhac, I., & Croitor, L. (2022). Dihydrazone Schiff base ligands–appropriate chemosensors for Cd (II)

detection. *Inorganic Chemistry Communications*, *146*, 110199. https://doi.org/10.1016/j.inoche.2022.110199.

11. Amin, Z., Rauf, T., Jan, Q., Kuchey, M. Y., Sofi, F. A., Ismail, T., ... & Bhat, M. A. (2023). Synthesis of a novel hydrazone functionality based spectrophotometric probe for selective and sensitive estimation of toxic heavy metal ions. *ChemistrySelect*, *8*(2), e202202632. https://doi.org/10.1002/slct.202202632.

12. Wu, M., Yang, D. D., Zheng, H. W., Liang, Q. F., Li, J. B., Kang, Y., ... & Jin, L. P. (2021). A multi-binding site hydrazone-based chemosensor for Zn (II) and Cd (II): a new strategy for the detection of metal ions in aqueous media based on aggregation-induced emission. *Dalton Transactions*, *50*(4), 1507-1513. https://doi.org/10.1039/D0DT04062B.

13. Xu, Q., Qin, W., Qin, Y., Hu, G., Xing, Z., & Liu, Y. (2024). A ratiometric fluorescence probe for visualized detection of heavy metal cadmium and application in water samples and living cells. *Molecules*, *29*(22), 5331. https://doi.org/10.3390/molecules29225331.

14. Wang, Z., Zheng, C., Xu, D., Liao, G., & Pu, S. (2022). A fluorescent sensor for Zn2+ and Cd2+ based on a diarylethene derivative with an indole-2-methylhydrazone moiety. *Journal of Photochemistry and Photobiology A: Chemistry*, *424*, 113634. https://doi.org/10.1016/j.jphotochem.2021.113634.